JOURNAL OF THERMOPHYSICS AND HEAT TRANSFER
Vol. 15, No. 4, October–December 2001

Microfilter Simulations and Scaling Laws

David R. Mott,* Elaine S. Oran,† and Carolyn R. Kaplan,‡
U.S. Naval Research Laboratory, Washington, DC 20375

A series of direct simulation Monte Carlo calculations of flows through microfilters were performed to evaluate the range of validity of a previously derived scaling law. This scaling law, which describes how the pressure drop across a filter depends on the Reynolds number and filter geometry, is based on Navier–Stokes calculations and experiments in the continuum regime. The simulations show that this scaling law predicts the correct Reynolds number dependence for a fixed Knudsen number, but the magnitude of the pressure drop is overpredicted as effects due to collisional nonequilibrium become important. The results of the simulations were used to derive a correction term to the scaling law that includes the Knudsen number and, thus, accounts for nonequilibrium effects.

Nomenclature

d	=	hole diameter
f	=	scaling factor based on Knudsen number
K	=	nondimensional pressure drop
Kn	=	Knudsen number, λ/L
K'	=	rescaled pressure drop defined by Eq. (15)
L	=	characteristic length
p	=	pressure
Re	=	Reynolds number
t	=	filter thickness
U	=	fluid velocity
$\bar{u}$	=	average fluid velocity
x, y	=	Cartesian coordinates
α	=	entrance effect parameter in Eq. (7)
β	=	opening factor
λ	=	mean free path
μ	=	viscosity
ρ	=	density

Subscripts

in	=	inflow value
out	=	outflow value
x	=	coordinate direction

Introduction

FILTERS and screens are commonly used in a wide variety of engineering applications, from isolating particulates in a gas sample to controlling turbulence levels in a wind tunnel. Because isolating particulates such as bioagents and airborne pathogens is now so important, we need to fabricate reliable filters with micrometer and submicrometer apertures.

When the particulates appear in very low concentrations, a relatively large amount of air must be filtered to get a sufficient sample. Because the power requirement for such a filtering procedure is the product of the flow rate and the pressure drop across the filter, obtaining an adequate sample becomes increasingly more expensive as the target particles become more dilute. An efficient filter design minimizes this pressure drop to reduce this expense.

Received 2 January 2001; revision received 3 May 2001; accepted for publication 3 May 2001. This material is declared a work of the U.S. Government and is not subject to copyright protection in the United States.

*Research Aerospace Engineer, Laboratory for Computational Physics and Fluid Dynamics, Code 6404; mott@lcp.nrl.navy.mil. Senior Member AIAA.

†Senior Scientist for Reactive Flow Physics, Laboratory for Computational Physics and Fluid Dynamics, Code 6404. Fellow AIAA.

‡Research Chemical Engineer, Laboratory for Computational Physics and Fluid Dynamics, Code 6410. Senior Member AIAA.

To predict performance and ultimately improve efficiency, there has been a significant effort over the years to quantify the relationship between filter performance and some set of global geometric parameters and flowfield conditions.[1,2] These studies led to scaling laws, which are algebraic expressions that indicate how the pressure drop across a screen or filter scales with system parameters. Such scaling laws can be used to optimize a filter design for a set of operating conditions as well as predict off-design performance of the filter. Scaling laws also provide a component model for a microfilter that can be used in system-level design and analysis of complex microfluidic systems.

This paper describes a series of direct simulation Monte Carlo (DSMC)[3] calculations used to quantify the relationship between power consumption and flow rate for filters in the high Knudsen number regime. The Knudsen number, defined as

$$Kn \equiv \frac{\text{mean free path}}{\text{characteristic length}} = \frac{\lambda}{L} \tag{1}$$

is a measure of the degree to which the flow deviates from equilibrium when there are too few molecular collisions. These effects appear for $Kn \gtrsim 0.01$, and Oran et al.[4] describe several methods for simulating flows in this regime. Navier–Stokes equations, which are based on the continuum approximation that assumes collisional equilibrium, may be used effectively up to $Kn \approx 0.1$ by incorporating slip boundary conditions.[5] However, the Navier–Stokes equations do not form a closed set unless the sheer stress and heat conduction can be written in terms of the lower-order macroscopic quantities.[3] These constitutive relationships, such as the relationship between viscous forces and strain rate, are only valid if there are enough intermolecular collisions. Therefore, the Navier–Stokes equations cannot be used when the system is too far from collisional equilibrium, regardless of the choice of boundary conditions. This breakdown occurs around $Kn \approx 0.1$ (Refs. 3 and 5).

The DSMC method[3] is a statistical approach for solving rarefied flow problems that does not rely on the constitutive assumptions required in Navier–Stokes calculations. In DSMC, a group of representative molecules are tracked as they move and collide. The essential approximation that differentiates DSMC methods from other particle methods is the assumption that the molecular movement and the collision calculations can be done independently. Each molecule moves independently over a given time step based on its velocity, and then a set of collisions are calculated between molecules that are relatively close after the move. The number of molecular collisions imposed on the system is given by the expected number of collisions in the real gas based on the time step, grid size, and flow conditions.

The simulations described here were used to modify a previously derived scaling law[6,7] to account for high Knudsen numbers. These results expand the range in which these expressions can be used to predict filter performance.

Scaling Laws for Filters and Screens

Early work on scaling laws for filters was inspired by the use of screens to control wind-tunnel turbulence. These screens generally consisted of round wires joined to form a grid. The pressure drop for such a grid can be estimated by assuming each wire acts as an independent, infinite cylinder.[1] Each wire sees a higher velocity than the inflow velocity approaching the screen due to a blockage effect. In other words, the screen occupies part of the channel, so that the flow must accelerate above the inflow velocity to maintain a given mass flux. These studies yielded empirical relationships between pressure drop and flow rate in terms of two geometric parameters and one flow parameter: the ratio of hole area to filter area (which is called the opening factor β), the ratio of filter thickness to hole diameter t/d, and the Reynolds number Re given by

$$Re = \rho_{\text{in}} U_{\text{in}} d/\beta\mu_{\text{in}} \tag{2}$$

The density, velocity, and viscosity of the inflow are ρ_{in}, U_{in}, and μ_{in}, respectively. This definition of Reynolds number includes the blockage effect of the filter by scaling U_{in} by β. Using the effective flow through the filter holes in the definition for Reynolds number improves the correlation of results for various hole geometries and flow conditions.[2] The earliest experimental work that resulted in scaling laws in terms of β, t/d, and Re was done at Reynolds number much larger than the conditions and filters of current interest.[1,2]

The actual filters on which the present study is based are more like a perforated plate than a wire mesh, but β, Re, and t/d are still the appropriate parameters for characterizing the pressure drop.[2] To illustrate this, and to develop a functional form for the scaling law, we first assume that each orifice is circular with fully developed flow throughout. The result for Hagen–Poiseuille flow that describes fully developed flow in a circular pipe provides the average velocity $\bar{u}$ in each channel as a function of pressure gradient, tube diameter, and viscosity (see Ref. 8),

$$\bar{u} = \frac{d^2}{32\mu}\left(-\frac{\mathrm{d}p}{\mathrm{d}x}\right) \tag{3}$$

We are interested in the pressure drop, $\Delta p = p_{\text{in}} - p_{\text{out}}$, across a filter of thickness t, and so we rewrite the pressure gradient as

$$-\frac{\mathrm{d}p}{\mathrm{d}x} = \frac{\Delta p}{t} \tag{4}$$

Assuming the flow is incompressible, we can relate the average velocity $\bar{u}$ to U_{in} using the opening factor:

$$\bar{u} = U_{\text{in}}/\beta \tag{5}$$

Substitution into Eq. (3) yields the following expression for Δp normalized by the incoming dynamic pressure:

$$K \equiv \frac{\Delta p}{\frac{1}{2}\rho U_{\text{in}}^2} = \beta^{-2}\frac{64}{Re}\frac{t}{d} \tag{6}$$

Here, K is the nondimensional pressure drop.

Therefore, if we assume the flow through each hole in the perforated plate is incompressible and fully developed without entrance or exit effects, the pressure drop is inversely proportional to β^2 and Reynolds number Re and directly proportional to t/d. The scaling law given by Eq. (6) would apply to filters with large t/d, for which entrance and exit effects are less significant, but for d large enough that Knudsen number effects are not important. We will now examine how the form of Eq. (6) changes as additional physical effects are included.

Schetz[9] presents solutions for pipe flow that include entrance effects, giving the following expression for the pressure drop across the filter once opening-factor effects are included:

$$K = \beta^{-2}[(64/Re)(t/d) + \alpha] \tag{7}$$

The additional term that appears in Eq. (7) but not in Eq. (6) accounts for friction in the developing region. A control-volume analysis provides an analytical form for α, and experiments indicate that $\alpha \approx 1.25$ is a reasonable approximation.[9] Equation (7) assumes that the flow becomes fully developed at some point in the channel and is not affected by exit effects, and so its potential usefulness as a scaling law is only slightly greater than Eq. (6).

Dagan et al.[10] provide a creeping-flow solution for a single finite length orifice that includes both entrance and exit effects. Their exact infinite series solution demonstrates that entrance and exit effects can be approximated using a linear term in t/d,

$$K = \beta^{-2}[(16/\pi)(t/d) + 3](4\pi/Re) \tag{8}$$

This approximation is a combination of Hagen–Poiseuille flow within the orifice and the solution for flow through an orifice in an infinitely thin wall. Unlike Eq. (7), Eq. (8) retains the correct Reynolds number dependence in the limit as $t \to 0$. However, at the scales currently of interest, this approximation does not provide accurate predictions.

Most recently, experimental and computational studies have been conducted in the continuum regime for filters with circular holes with diameters from 5 to 12 μm (Refs. 6, 7, and 11), which is well outside the parameter range of earlier work on filter scaling laws. Based on these studies, Yang et al.[6] suggested a scaling law that has the general form developed in the preceding paragraphs, but has empirical constants in each of the terms,

$$K = \beta^{-2}[3.5(t/d) + 3][(10/Re) + 0.22] \tag{9}$$

Here, K is inversely proportional to β^2 and linear in t/d as in Eq. (8), but now it is also linear in $1/Re$ rather than being directly proportional to this parameter.

Yang et al.[6] developed Eq. (9) using solutions to the incompressible Navier–Stokes equations and then compared these to experimental results. The calculations included noncontinuum effects in the form of a slip boundary condition at the filter surface, but these effects were minor for the cases tested. Rather than include an additional parameter such as Knudsen number in the scaling law, the relatively small nonequilibrium effect was incorporated into the values of the constants in Eq. (9).

Filters for biodetection, however, require holes that are even smaller than those tested by Yang et al.[6,11] A rod-shaped anthrax spore, for example, is generally 4.5–10 μm long by 1–1.5 μm across. As hole diameters are reduced to 1 μm or less, Knudsen number effects will be substantial. These effects must then be included explicitly in the scaling law.

Gombosi[12] provides an analysis of pipe flow that includes slip effects. Using the mean free path method of gas kinetics, he shows that the standard Hagen–Poiseuille result given in Eq. (6) can be scaled to include slip effects by a term involving Knudsen number. His analysis applied to the microfilter problem gives the expression

$$K = \beta^{-2}(64/Re)(t/d)[1 + (16/3)Kn]^{-1} \tag{10}$$

The constant $\frac{16}{3}$ is not empirical, but comes from the gas kinetic analysis. In the continuum limit, $Kn \to 0$, and Eq. (10) approaches Eq. (6). As Knudsen number increases from zero, the pressure drop decreases due to the effects of slip at the channel walls. Beskok et al.[5] show that this linear term in Knudsen number overpredicts the effects of slip, and they present a higher-order slip boundary condition that includes a Kn^2 term. However, we are interested in adding a simple correction to the scaling law given in Eq. (9), and so the linear form is preferred. The form of this correction factor for including Knudsen number effects in the Hagen–Poiseuille result foreshadows the correction that will be added to Eq. (9) to include Knudsen number effects in the microfilter scaling law.

Note that these scaling laws do not include compressibility effects, which can be significant in microflows.[5] The framework developed here is used to derive a correction to Eq. (9) that incorporates Knudsen number effects, and limitations of this framework are discussed in more detail in conjunction with the results of the study.

Numerical Approach

Two-dimensional DSMC calculations were first performed for the baseline geometry described in Fig. 1 using the parameters listed in Table 1. Parameter studies were performed by varying the flow

Table 1 Simulation parameters for baseline calculation

Parameter	Value
t/d	3
β	0.25
Kn	0.0576
Re	0.96
Mass flow	4.89 kg/m^{2}s
Ratio of real to simulated particles	10^{10}
Sampling cell length	$1.72\lambda_{in}$
Average molecules per sampling cell	25
Collision cell length	$0.86\lambda_{in}$
Time step	5×10^{-11} s
Time step/mean collision time of inflow	0.43
Time steps to steady state	100,000
Time steps between samples at steady state	5
Samples taken at steady state	100,000

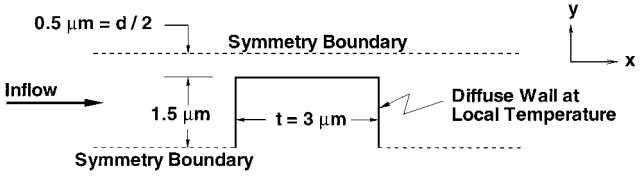

Fig. 1 Geometry of baseline case.

conditions and geometry relative to this case. The baseline case consists of a filter 3 μm thick with 1-μm holes spaced 4 μm apart. These dimensions give $t/d = 3$ and $\beta = \frac{1}{4}$. For the current studies, we fix β and t/d, so that variations in the results are limited to Reynolds number and Knudsen number effects. The computational domain is effectively reduced by exploiting planes of symmetry along the centerline of a filter hole and along the boundary between adjacent holes. The inflow conditions are air at roughly sea-level temperature and density, flowing at 4.89kg/(m^{2}s) toward the filter from the left. The Knudsen number is defined as

$$Kn = \lambda_{in}/d \tag{11}$$

in terms of the mean free path of the inflow, λ_{in}. For the baseline conditions, $Kn = 0.0576$.

The calculations were performed with a modified version of DSMC2.FOR.[3] The modifications allow the user to include an arbitrary number of surfaces within the domain and impose an adiabatic, diffuse-reflection condition at a surface. Half of one orifice is then modeled using a step-shaped blockage as shown in Fig. 1. DSMC requires defining a ratio of real to simulated particles, here taken as 10^{10}, and a computational grid, here established with 100 (square) computational cells per 1 μm^2. These choices give approximately 25 simulated molecules per computational cell. The time step for the baseline case was 5×10^{-11} s, so that a molecule moving at the root mean square molecular speed travels about one-quarter of a cell width during a time step. Each cell was divided into four square subcells for determining collision partners, and each edge on these subcells was approximately $0.86\lambda_{in}$. These code parameters were chosen to provide adequate resolution of the flowfield and convergence of the statistical quantities, and these parameters were varied to verify the accuracy of the simulations.

To control the Reynolds number from case to case, the mass flux through the domain was specified by the inflow conditions. During a time step, the number of molecules that exited across the inflow boundary were counted, and then molecules were added at the inflow to satisfy the specified mass flux. The velocity for each incoming molecule was set using a prescribed temperature and mean velocity, although the prescribed mean velocity is much smaller than the mean thermal velocity for the cases studied. For the baseline case, this prescribed mean velocity is 4 m/s, as compared to a mean thermal velocity of 496 m/s.

Molecules also enter the domain across the downstream boundary. These molecules were taken from a prescribed distribution defined by a specified velocity, density, and temperature. Because this condition overspecifies the subsonic outflow, the solution close to the exit plane adjusts in an attempt to resolve the inconsistency. In other words, a smooth but pronounced transition occurs in the cells close to the end of the domain from the constant state downstream of the microfilter to an exit state more compatible with the overspecified boundary values. To ensure that this transition region did not affect the computed pressure drop, the downstream boundary was placed far enough downstream. Extensive tests in which the domain length was varied show that imposing the downstream boundary condition approximately $10t$ from the filter prevents this inconsistency from affecting the solution near the filter.

Results and Discussion

Baseline Results

Contour maps of the x velocity, u_x, and ρ for the baseline case are shown in Figs. 2 and 3. The map of u_x shows that the flow accelerating through the hole reaches a maximum speed of ~24 m/s along the hole centerline. There is also a distinct boundary-layer structure in the channel. The density increases slightly (~2%) upstream of the filter, a ram effect produced by forcing the flow through at a specified mass flux. The flow then expands as it moves through the filter. The final density value downstream of the channel exit is ~10% below that of the incoming flow.

Figure 4 shows profiles of p, u_x, and ρ along the centerline of the channel. The noise in these profiles arises because DSMC is a stochastic method, but with this small amount of noise, no special techniques are required to determine the solution. The values of pressure in front of and behind the filter can be identified, so that we can evaluate the Δp predicted by the scaling laws.

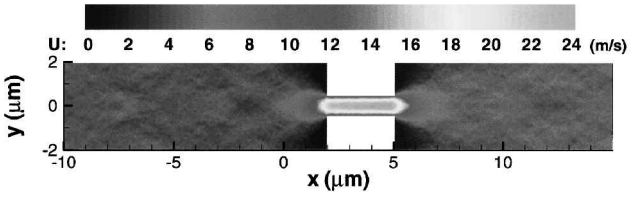

Fig. 2 Contours of x velocity for baseline case.

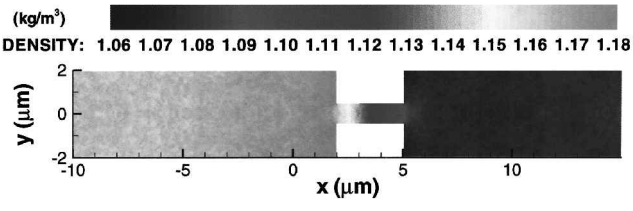

Fig. 3 Density contours for baseline case.

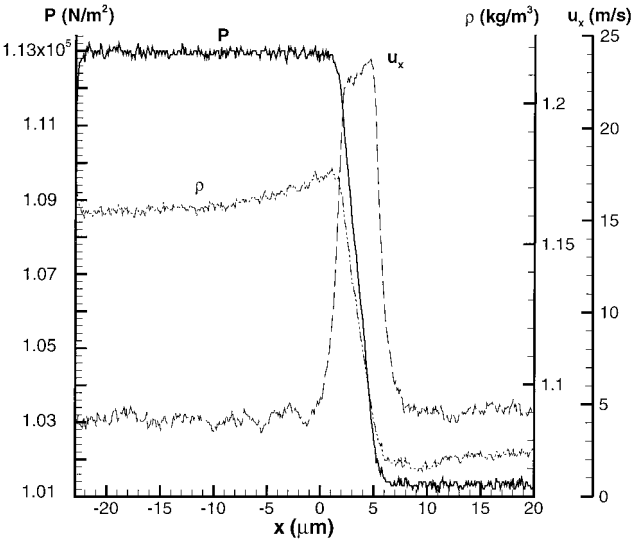

Fig. 4 Centerline pressure, velocity, and density for baseline case.

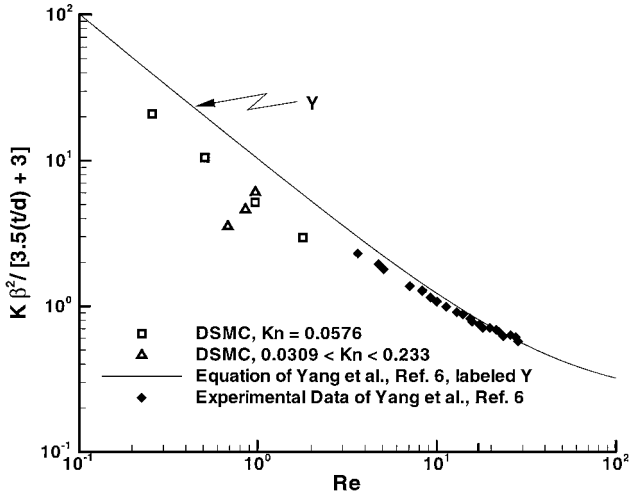

Fig. 5 Nondimensional pressure drop for various cases, including DSMC calculations, experimental results,[6] and Yang et al. empirical fit[6] given in Eq. (9).

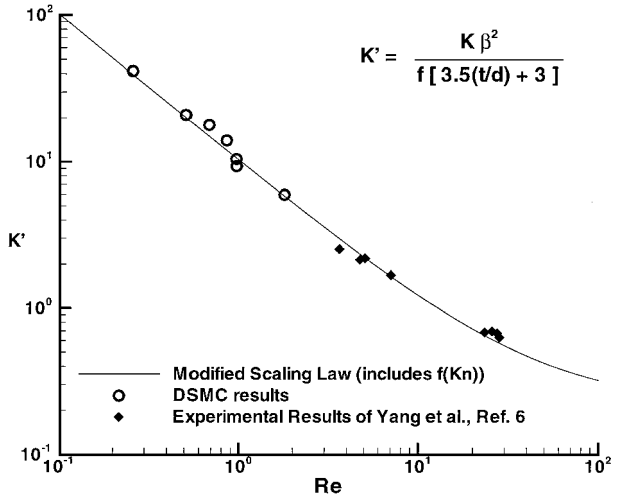

Fig. 6 Comparison of DSMC results with scaled empirical fit given in Eq. (12); experimental results from Yang et al.[6] are also included.

Parameter Studies

The results of the baseline and several other cases obtained by varying the flow conditions and geometry are shown in Fig. 5, which also includes the Yang et al. scaling law [Eq. (9)],[6] labeled Y, and some of their experimental data.[6] The experimental data are in the range $0.0057 \leq Kn \leq 0.0127$. The squares represent data for constant $Kn = 0.0576$ as defined in Eq. (11). These points lie below Y by around a factor of 2. The experimental data lie below Y as well at low Reynolds number, but the DSMC data disagree with Y more strongly. As Knudsen number increases, slip effect become more pronounced, reducing the pressure drop for a given Reynolds number. Therefore, the DSMC results lie below the trend seen in the experimental data taken at lower Knudsen number.

The triangular data points in Fig. 5 correspond to simulations with $Kn = 0.0309$, 0.117, and 0.233. The $Kn = 0.0309$ data point is closest to Y, the $Kn = 0.233$ data point is the farthest from Y, and the $Kn = 0.117$ point is in the middle. This ordering is expected because as Knudsen number increases, slip effects increase, reducing the pressure drop. Furthermore, these points indicate that the dependence of K on Knudsen number is substantial. Consider the triangular point farthest from Y, for which $Kn = 0.233$ and $Re = 0.68$. If K showed no dependence on Knudsen number, this point would fall in line with the $Kn = 0.0576$ data, which is not the case. The value of K interpolated at $Re = 0.68$ from the $Kn = 0.0576$ data is approximately three times that given by the simulation for $Kn = 0.233$ at the same Reynolds number. The scaling law predicts a single value of K at this Reynolds number, regardless of the value of Knudsen number that is over four times the value obtained for $Kn = 0.233$ using DSMC.

Can we include a factor in Eq. (9) to account for this reduction in K as Knudsen number increases? If we base this factor f on Knudsen number and include it as

$$K = f\beta^{-2}[3.5(t/d) + 3][(10/Re) + 0.22] \tag{12}$$

we must require f to satisfy

$$f(Kn = 0) = 1, \qquad \frac{\partial f}{\partial Kn} < 0 \tag{13}$$

In other words, the scaling law should return the continuum limit as $Kn \to 0$, and f decreases as Knudsen number increases from $Kn = 0$. An expression that satisfies both of these requirements and has only one free parameter is

$$f = a/(a + Kn) \tag{14}$$

This is the form for f given by the mean free path method and shown in Eq. (10), with $a = \frac{3}{16}$. However, the fixed form of Eq. (9) prevents it from returning the exact Hagen–Poiseuille solution as $t/d \to \infty$. Therefore, to use Eq. (9), we determine a by matching the calculated results to Eq. (12). Because we have several data points but only one free parameter, we choose a to minimize the sum of the differences between the prediction given by Eq. (12) and the simulation data. This procedure gives $a = 0.0577$.

The data points from Fig. 5 are shown in Fig. 6 in a new format that removes the Knudsen number dependence. The abscissa K' is given by

$$K' \equiv \frac{K\beta^2}{f\,(3.5\,t/d + 3)} \tag{15}$$

which is the abscissa in Fig. 5 scaled by $1/f$. This scaling removes variation due to Knudsen number, projecting the results to an equivalent $Kn = 0$ value. Therefore, the Yang et al.[6] curve appears unchanged in Fig. 6, and if the Knudsen number scaling is accurate, then all of the data points should lie on this curve.

The scaling shown in Fig. 6 has much less scatter than that in Fig. 5. The scaled DSMC results at the highest and lowest Knudsen number values miss the empirical curve by around 15%, which is a substantial improvement over the factor of 2–5 difference seen for the unscaled results. Because only one free parameter, a, was available for matching all of the DSMC data to the empirical curve, the agreement is very good.

A more challenging test of the scaling law is provided by the Yang et al. data,[6] some of which are also included in Fig. 6. These data were not used to determine a for Eq. (14). The density of these data as presented in Ref. 6 makes it difficult to identify the case, that is, Knudsen number, corresponding to every individual data point, and so only a few unambiguous points at the lowest and highest Reynolds number values presented in Ref. 6 are included. Therefore, the Knudsen number is known for each data point included in Fig. 6, and each point is scaled using f. Before scaling, the low Reynolds number data in Ref. 6 differed from the empirical curve by 16–23%. After scaling, this error is reduced to 0.3–16%. However, the data points at the highest Reynolds number reported in Ref. 6 are closer to the empirical curve before to the f scaling. Errors in the range of 0.5–4.5% for the unscaled data increase to 5.4–15% after scaling. Because Eq. (9) incorporated Knudsen number effects into its empirically determined constants, better agreement over this entire range of Reynolds number may be achieved by reexamining the data used to derive Eq. (9) and isolating the Knudsen number effect in f. Overall, however, the scaling law performs very well.

The data points for the $Kn = 0.117$ and 0.233 cases lie above the curve in Fig. 6 given by the new scaling law, which indicates that the scaling law underpredicts the pressure drop required to sustain the flow under those conditions. In contrast, the data point corresponding to $Kn = 0.0309$ lies below the curve for the new scaling law, and so the scaling law overpredicts the pressure drop required. Therefore, the pressure drop is underpredicted for the cases with highest

Knudsen number, and it is overpredicted for the lowest Knudsen number. This result has two causes. As mentioned earlier, Beskok et al.[5] demonstrate that a standard correction for slip flow comparable to the correction seen in Eq. (10) overpredicts the effects of slip. They include a second-order term in Knudsen number that reduces this effect, which would appear in Eq. (14) as

$$f = a/(a + Kn - bKn^2) \tag{16}$$

with $b > 0$. Adding such a term and adjusting the value of a would allow the scaling law to more accurately match the DSMC results, but the usefulness in doing this is unclear. The scaling law is meant to be an engineering tool, and the primary effects of collisional nonequilibrium are captured by the linear Knudsen number term. Additional effects that are not considered by the scaling law should be explored before refining the Knudsen number based correction.

Compressibility is important in microflows[5] and also contributes to the trends seen in the DSMC data. The scaling law given in Eq. (9) is based on incompressible computations, and the form of f given in Eq. (14) is based on incompressible theory. The cases with the highest Knudsen number in the current study were realized by decreasing the filter hole size and increasing the velocity, which kept Reynolds number within a narrow range but increased the role of compressibility. The lower Knudsen number data point was obtained by increasing the hole size and decreasing the velocity, reducing the effects of compressibility.

As shown in Ref. 5, compressibility reduces the mass flow below that expected of an incompressible flow experiencing the same pressure drop. In other words, a higher pressure drop is required to support a given mass flow rate as compressibility becomes significant. Therefore, the current results are consistent with the role of compressibility seen in previous studies. The more compressible cases require a higher pressure drop than expected based on the scaling law, and the least-compressible case does not require as much of a pressure drop to support the flow. This argument seems to imply that the scaling law should underpredict the pressure drop for all of the DSMC results because some degree of compressibility is seen in even the low Knudsen number cases. However, a was chosen to best fit the DSMC results, and so the effects of compressibility are included in f to some degree.

Additional studies could be performed to determine if differences between the scaling law and the experimental data may also be attributed in part to compressibility. Nonetheless, Figs. 5 and 6 suggest that the correction included in Eq. (12) based on Knudsen number is of primary importance in reconciling the high Knudsen number data with the scaling law, and in the current range of parameters, compressibility is of secondary importance.

Conclusions

As microfilters are fabricated with smaller and smaller holes, noncontinuum effects will become more important. The scales required for filtering bioagents of current interest experience strong Knudsen number effects, which requires an extension of the classic scaling laws used to predict filter performance. Based on current calculations, this scaling law is

$$K = \beta^{-2}\left(3.5\frac{t}{d} + 3\right)\left(\frac{10}{Re} + 0.22\right)\left(\frac{0.0577}{0.0577 + Kn}\right) \tag{17}$$

When the factor based on the Knudsen number is included, a reasonable adjustment can be made in the pressure-drop calculation that is within about 15% of the solutions calculated in the current study using the DSMC method. This scaling reduces the error in predicting previous low Reynolds number experimental data from the range 16–23% to 0.3–15%. However, the scaling increased the error in the correlation from 0.5–4.5% to 5.4–15% at higher Reynolds number.

Improved accuracy over a wide range of Reynolds numbers may be achieved by reexamining the data that led to Eq. (9) and isolating the effects of Knudsen number in f, as well as through additional studies in which the effects of collisional nonequilibrium and surface slip are separated from the effects of compressibility. Further development of Eq. (17) should also continue based on three-dimensional simulations. Two-dimensional simulations were pursued here because the same functional form seen in Eq. (6) for three-dimensional Poiseuille flow holds for two-dimensional flow through a channel of width d (Ref. 8). Also, the form of f in Eq. (14) follows the form of the three-dimensional correction term suggested by Gombosi.[12] The value obtained for a in Eq. (14) by matching the current two-dimensional calculations successfully correlates the low Reynolds number data of Yang et al.,[6] but a may need adjusting based on three-dimensional simulations, especially if the constants in Eq. (9) were adjusted to isolate Knudsen number effects in f.

Acknowledgments

This work is funded by the Defense Advanced Research Projects Agency Design for Mixed Technology Integration Program. This work was performed while D. Mott held a National Research Council–Naval Research Laboratory Research Associateship. The authors would like to thank Chih-Ming Ho and Yu-Chong Tai for suggesting this problem and, along with Joon Mo Yang, for discussing their results with us.

References

[1] Wieghardt, K. E. G., "On the Resistance of Screens," *Aeronautical Quarterly*, Vol. 4, Feb. 1953, pp. 186–192.

[2] Derbunovich, G. I., Zemskaya, A. S., Repik, Ye. U., and Sosedko, Yu. P., "Hydraulic Drag of Perforated Plates," *Fluid Mechanics—Soviet Research*, Vol. 13, No. 1, 1984, pp. 111–116.

[3] Bird, G. A., *Molecular Gas Dynamics and the Direct Simulation of Gas Flows*, Oxford Univ. Press, Oxford, England, U.K., 1994.

[4] Oran, E. S., Oh, C. K., and Cybyk, B. Z., "Direct Simulation Monte Carlo—Recent Advances and Applications," *Annual Review of Fluid Mechanics*, Vol. 30, 1998, pp. 403–441.

[5] Beskok, A., Karniadakis, G. E., and Trimmer, W., "Rarefaction and Compressibility Effects in Gas Microflows," *Journal of Fluids Engineering*, Vol. 118, No. 3, 1996, pp. 448–456.

[6] Yang, J. M., Yang, X., Ho, C.-M., and Tai, Y.-C., "Prediction of the Pressure Drop Through Micromachined Particle Filters," *Technical Proceedings of the International Conference on Modeling and Simulation of Microsystems (MSM'99)*, Applied Computational Research Society, Cambridge, MA, 1999, pp. 546–549.

[7] Yang, J. M., Yang, X., Ho, C.-M., and Tai, Y.-C., "Micromachined Particle Filter with Low Power Dissipation," *Journal of Fluids Engineering* (to be published).

[8] White, F. M., *Viscous Fluid Flow*, 2nd ed., McGraw–Hill, New York, 1991, pp. 116–119.

[9] Schetz, J. A., *Boundary Layer Analysis*, Prentice–Hall, Englewood Cliffs, NJ, 1993, pp. 317, 318.

[10] Dagan, Z., Weinbaum, S., and Pfeffer, R., "An Infinite-Series Solution for the Creeping Motion Through an Orifice for Finite Length," *Journal of Fluid Mechanics*, Vol. 115, 1982, pp. 505–523.

[11] Yang, X., Yang, J. M., Tai, Y.-C., and Ho, C.-M., "Micromachined Membrane Particle Filters," *Sensors and Actuators A: Physical*, Vol. 73, No. 1–2, 1999, pp. 184–191.

[12] Gombosi, T. I., *Gaskinetic Theory*, Cambridge Univ. Press, Cambridge, England, U.K., 1994, p. 142.